International Journal of Vehicle Safety

ISSN online: 1479-3113 - ISSN print: 1479-3105
https://www.inderscience.com/ijvs

Multi-objective optimisation design and fuzzy PID control for racing car variable rear wing system

Xinxin Kong, Zhaowen Deng, Sijia Yu, Wei Gao, Baohua Wang

DOI: 10.1504/IJVS.2022.10054756

Article History:
Received: 25 January 2022
Accepted: 07 March 2022
Published online: 17 March 2023

Multi-objective optimisation design and fuzzy PID control for racing car variable rear wing system

Xinxin Kong

College of Automotive Engineering,
Hubei University of Automotive Technology,
Shiyan, Hubei, China
Email: 805205005@qq.com

Zhaowen Deng*

College of Automotive Engineering,
Hubei University of Automotive Technology,
Shiyan, Hubei, China
and
College of Energy and Power Engineering,
Nanjing University of Aeronautics and Astronautics,
Nanjing, Jiangsu, China
Email: dengzw_qc@huat.edu.cn
*Corresponding author

Sijia Yu

College of Automotive Engineering,
Hubei University of Automotive Technology,
Shiyan, Hubei, China
Email: 1137069821@qq.com

Wei Gao

College of Automotive Engineering,
Hubei University of Automotive Technology,
Shiyan, Hubei, China
and
College of Energy and Power Engineering,
Nanjing University of Aeronautics and Astronautics,
Nanjing, Jiangsu, China
Email: 347825162@qq.com

Baohua Wang

College of Automotive Engineering,
Hubei University of Automotive Technology,
Shiyan, Hubei, China
Email: wbhbenz@126.com

Abstract: To improve the aerodynamic characteristics of the rear wing and enhance the handling stability of the racing car, based on the orthogonal experimental design and iSIGHT platform, the multi-objective optimisation of the structural parameters of the spatial layout of the rear wing was carried out to determine the optimal combination of the angle of attack between the rear wings and the clearance between adjacent wings. A hybrid fuzzy PID variable rear wing control system was developed to suppress vehicle roll by real-time control of the flap angle of attack. The co-simulation results show that as the road adhesion coefficient decreases, the variable rear wing system improves the handling stability of the car more and more and the suppression of vehicle roll gradually increases, with the improved handling stability on slippery roads, the car's cornering performance and driving safety are enhanced.

Keywords: variable rear wing; active aerodynamic system; pneumatic characteristics; orthogonal experiments; multi-objective optimisation; fuzzy PID.

Reference to this paper should be made as follows: Kong, X., Deng, Z., Yu, S., Gao, W. and Wang, B. (2022) 'Multi-objective optimisation design and fuzzy PID control for racing car variable rear wing system', *Int. J. Vehicle Safety*, Vol. 12, Nos. 3/4, pp.281–306.

1 Introduction

Formula SAE has grown rapidly around the world due to its design autonomy and innovation (Yu and Xie 2018). The development of Computational Fluid Dynamics (CFD), wind tunnel tests, numerical simulation techniques and active safety technologies has contributed to the development of racing car aerodynamics (Liu, 2018; Zhu, 2017). The Active Aerodynamics Control System can significantly improve the aerodynamic characteristics of the car, enhancing cornering performance and handling stability under extreme conditions (Diba et al., 2017). Yang et al. (2011) proposed a method for optimising the aerodynamic design of the rear wing of a racing car, and through computer programming, the modelling and numerical calculation of the rear wing were implemented to improve the computational efficiency, resulting in an optimised solution with 6% more lift and 5% less aerodynamic drag than the initial model. Ni et al. (2012) proposed a method that accounts for the aerodynamic characteristics of the rear wing in the dynamics simulation and compared the performance of the car when the rear wing took different angles of attack, and the results showed that the increase of the rear wing attack angle could improve the transient response performance and the side wind stability of the car. Deng et al. (2016) developed software and hardware for the adjustable wing control system based on embedded technology and realised the intelligent adjustable rear wing attack angle under different operating conditions through prototype tests. Zhang et al. (2018) designed a racing rear wing drag reduction system, which effectively improved the cornering driving stability of the racing car. He (2013) conducted CFD analysis and parametric study of the rear wing of a vehicle to design an active controller for the rear wing that can improve the vehicle handling performance and stability by controlling the angle of attack of the rear wing. Ayyagari and He (2017) independently controlled the

angle of attack of left and right spoilers, which could enable the rear end of the vehicle to obtain different left and right downforce and driving resistance, which was conducive to the implementation of active yaw and roll moment control of the vehicle and significantly improved the stability of high-speed vehicles. Dida et al. (2014) established a non-linear model of a racing car with a rear wing, controlled the rear wing attack angle variation by PID, and verified the effectiveness of the active rear wing control system by simulation analysis. Hammad et al. (2019) and Hammad (2019) applied linear-quadratic optimal control and sliding mode control theory to control the rear wing attack angle, respectively, to develop a disconnected variable rear wing control model, and verified the effectiveness of the active aerodynamic system based on simulations.

Existing research on variable rear wing systems mainly focuses on active control of rear wing attack angle, while less research considers both wing multi-objective optimisation and active control of rear wing attack angle. In this paper, based on the CFD simulation analysis of the whole vehicle, and based on the orthogonal experimental design and iSIGHT platform, the spatial layout structure parameters of the rear wing are correlated with its two evaluation indexes of lift and lift drag ratio, and the absolute values of lift and lift drag ratio are maximised as the target, and the optimal angle of attack variation range between the airfoils and the clearance between adjacent airfoils under the straight-line operating conditions are determined. To further improve the handling stability of the race car under turning conditions on wet roads, a variable rear wing control system was developed to suppress vehicle roll by controlling the flap angle of attack in real-time to generate different positive pressures on its left and right rear wheels. A hybrid fuzzy PID variable rear wing system control strategy is designed with the design objective of tracking the desired steady-state transverse swing angular velocity. Based on the joint simulation platform of Matlab/Simulink and CarSim, the effectiveness of the hybrid fuzzy PID variable rear wing control strategy is verified under the single shift line condition, the same vehicle speed and different ground adhesion coefficient conditions.

2 Racing car rear wing orthogonal experiment

2.1 Racing car rear wing modelling and spatial structure parameter determination

The aerodynamic kit, an important part of the racing body, consists of a front wing, a rear wing and a bottom diffuser. The rear wing, an important part of the aerodynamic package, provides approximately 40% of the downforce for the entire aerodynamic package (He et al., 2013). By optimising the design and precise control of the rear wing of the car, the handling stability of the car can be further improved.

The airfoil selection of the tailplane has a significant impact on the airflow flowing through the airfoil surface, and the shape of the airfoil section determines the area and size of the airfoil. The tailplane is mainly composed of the main wing, the first flap, the second flap and the endplate, and because the racing car has the characteristics of lower driving speed and more complicated operating conditions, the GOE 430 was finally selected as the main wing section and the GOE 441 as the flap section through Profile software analysis. Since the speed at which the racing car travels is generally 20 m/s

(Hu et al., 2015), the Reynolds number is chosen to be 600,000 and its lift drag ratio is maximised at an angle of attack of the main wing of approximately 5°. The effect of the main rear wing attack angle variation on lift drag ratio is shown in Figure 1.

Figure 1 Effect of change in angle of attack of the main wing on lift drag ratio

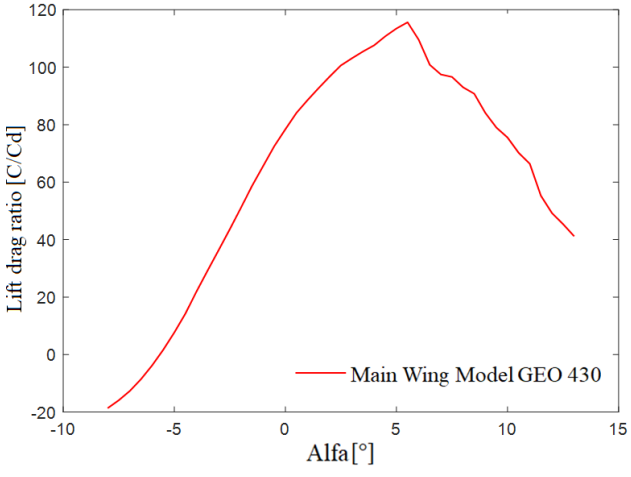

The selected wing shape is saved as a *.dxf file and imported into CATIA to establish a 3D model of the trailing wing. According to the race rules and to meet the requirements of the aerodynamic characteristics of the racing car (Li, 2015), the preliminary design of the rear wing dimensions are 350 mm in the length of the main wing chord and 1350 mm in width of the wingspan, 200 mm in the length of the first rear flap chord and 1350 mm in width of the wingspan, 160 mm in the length of the second rear flap chord and 1350 mm in width of the wingspan 1350 mm and the leading edge radius is 3 mm. The angle of attack of the main wing is 5°, the initial angle of attack of the first flap is 25° and the initial angle of attack of the second flap is 45°. The preliminary design of the three-dimensional model of the rear wing is shown in Figure 2.

Figure 2 3D model of the rear wing

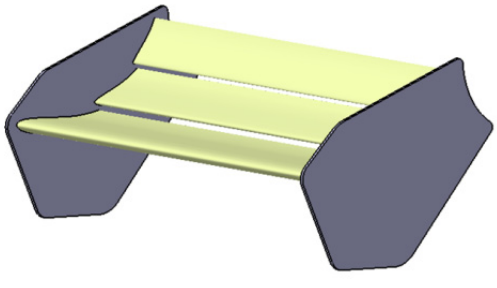

Since the main parameters affecting the aerodynamic characteristics of the tailplane are the angle of attack of the main flap, the relative clearance between the airfoils and the endplate position, the structural parameters of the angle of attack, and the relative spatial

position, which have a greater influence on the aerodynamic characteristics of the tailplane, are taken as design variables and the spatial structural parameters of the tailplane are $\theta_1, \theta_2, X_1, X_2, Y_1, Y_2$, under the premise that the angle of attack of the main wing is determined to be 5° and the three-dimensional model of the tailplane is parameterised. The specific position is shown in Figure 3. θ_1 is the angle of attack of the first flap, θ_2 is the angle of attack of the second flap, X_1 is the horizontal distance between the main flap and the first flap, X_2 is the horizontal distance between the first flap and the second flap, Y_1 is the vertical distance between the main flap and the first flap and Y_2 is the vertical distance between the first flap and the second flap.

Figure 3 Parameters of rear wing space structure

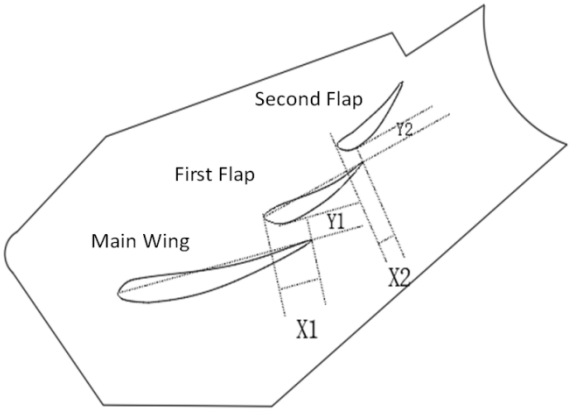

2.2 Design of orthogonal experiments for tailplane space parameters

In the optimal design of the rear wing space structure layout parameters, ignoring the influence of the endplate factor, only the design of the orthogonal table should be considered (Xu et al., 2009), according to the number of selected design parameters (6) and the number of horizontal number parameters (5), the orthogonal table is selected as $L_{25}\left(5^6\right)$, where 1, 2, 3, 4, 5, 6 are the different factors of the 6 design parameters, as shown in Table 1 and in ANSYS Work Bench to simulate and analyse one by one, the general speed of FSAE racing is in the range of 15—25 m/s (Wan, 2018; Xu et al., 2009), so a speed of 20 m/s is selected for the study, and the test results are recorded in Table 2.

Table 1 List of levels of each factor

Number of levels	θ_1 *(deg)*	θ_2 *(deg)*	X_1*(mm)*	Y_1*(mm)*	X_2*(mm)*	Y_2*(mm)*
1	10	20	22	8	12	6
2	15	30	24	10	14	8
3	20	40	26	12	16	10
4	25	50	28	14	18	12
5	30	60	30	16	20	14

Based on the calculated values obtained from the computational hydrodynamic simulations in Table 2, a table of response values and the main effects plot of the calculated values of lift force and lift resistance ratio was calculated. In the orthogonal experimental design, polar difference analysis is generally used to assess the order of importance of the experimental factors and the larger the polar difference, the greater the influence of the parameter on the test results (Wan, 2018).

Table 2 Orthogonal experiment assignment and results

Test number	*Wing space structure parameters*						*Calculated values*	
	θ_1	θ_2	X_1	Y_1	X_2	Y_2	*Liftoff value* (N)	*Lift drag ratio*
1	1	1	1	1	1	1	–290.434	–6.4539
2	1	2	3	4	5	2	–383.406	–5.6118
3	1	3	5	2	4	3	–440.315	–4.9511
4	1	4	2	5	3	4	–476.681	–4.5494
5	1	5	4	3	2	5	–452.339	–4.3223
6	2	1	5	4	3	5	–338.054	–6.6024
7	2	2	2	2	2	1	–398.975	–5.3916
8	2	3	4	5	1	2	–461.244	–4.7561
9	2	4	1	3	5	3	–512.035	–4.2980
10	2	5	3	1	4	4	–520.146	–4.0144
11	3	1	4	2	5	4	–348.221	–5.8015
12	3	2	1	5	4	5	–429.894	–5.1426
13	3	3	3	3	3	1	–474.354	–4.5941
14	3	4	5	1	2	2	–513.567	–4.1284
15	3	5	2	4	1	3	–571.744	–3.8702
16	4	1	3	5	2	3	–377.649	–5.6128
17	4	2	5	3	1	4	–440.882	–4.9148
18	4	3	2	1	5	5	–490.324	–4.3599
19	4	4	4	4	4	1	–539.574	–4.0158
20	4	5	1	2	3	2	–565.045	–3.7049
21	5	1	2	3	4	2	–394.554	–5.3336
22	5	2	4	1	3	3	–448.864	–4.7327
23	5	3	1	4	2	4	–517.258	–4.2177
24	5	4	3	2	1	5	–545.394	–3.8282
25	5	5	5	5	5	1	–571.742	–3.6119

Table 3 Response value of lift value

Number of levels	θ_1 *(deg)*	θ_2 *(deg)*	X_1 *(mm)*	Y_1 *(mm)*	X_2 *(mm)*	Y_2 *(mm)*
1	–408.6	–349.8	–462.9	–452.7	–461.9	–455
2	–446.1	–420.4	–466.5	–459.6	–452	–463.5
3	–467.6	–476.7	–460.2	–454.8	–460.6	–470.1
4	–482.7	–517.5	–450	–470	–464.9	–460.6
5	–495.6	–536.2	–460.9	–463.4	–461.1	–451.2
Range value	86.9	186.4	16.4	17.3	12.9	18.9

Table 4 Response value of lift drag ratio

Number of levels	θ_1 *(deg)*	θ_2 *(deg)*	X_1*(mm)*	Y_1*(mm)*	X_2*(mm)*	Y_2*(mm)*
1	–5.18	–5.96	–4.76	–4.74	–4.76	–4.81
2	–5.01	–5.16	–4.70	–4.74	–4.73	–4.71
3	–4.71	–4.58	–4.73	–4.69	–4.84	–4.69
4	–4.52	–4.16	–4.73	–4.86	–4.69	–4.70
5	–4.34	–3.90	–4.84	–4.73	–4.74	–4.85
Range value	0.833	2.056	0.141	0.171	0.145	0.158

To analyse the trend of lift value and lift-to-resistance ratio with the level of each factor, the horizontal coordinates of the level value of each factor and the vertical coordinates of the lift value and lift-to-resistance ratio were used, respectively, and the trend graphs of the influence of each factor on the lift value and lift drag ratio were obtained as shown in Figures 4 and 5.

Figure 4 The trend of the influence of various factors on the value of lift

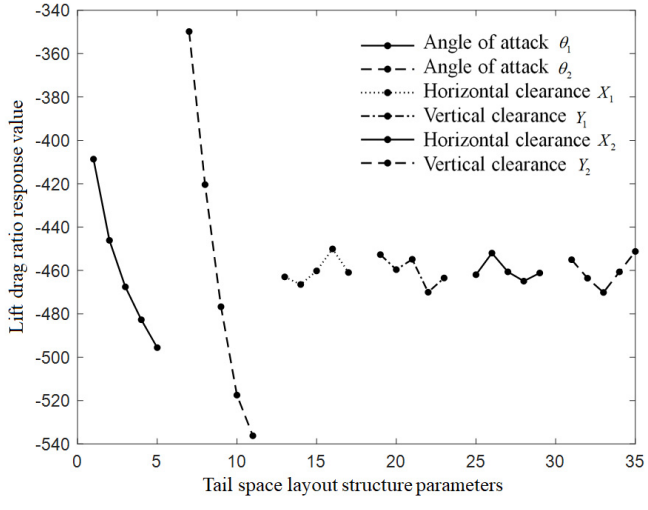

Figure 5 The trend of the influence of various factors on the lift drag ratio *L*/*D*

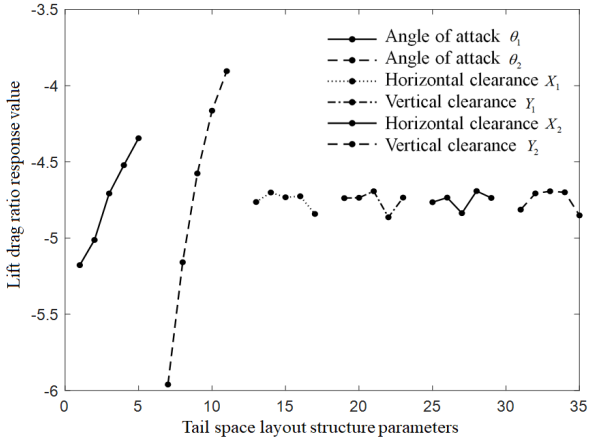

According to the extreme difference analysis, the order of influence of each factor on the lift value, second flap angle of attack $\theta_2 >$ first flap angle of attack $\theta_1 >$ vertical distance between the first flap and second flap $Y_2 >$ vertical distance between the main flap and the first flap $Y_1 >$ horizontal distance between the main flap and the first flap $X_1 >$ horizontal distance between the first flap and second flap X_2, and the order of influence of each factor on the lift-to-drag ratio is: second flap angle of attack $\theta_2 >$ first flap angle of attack $\theta_1 >$ vertical distance between the main flap and first flap $Y_1 >$ horizontal distance between the first flap and second flap X_1. The angle of attack of the second flap $\theta_2 >$ the angle of attack of the first flap $\theta_1 >$ the vertical distance between the main wing and the first flap $Y_1 >$ the vertical distance between the first flap and the second flap $Y_2 >$ the horizontal distance between the first flap and the second flap $X_2 >$ the horizontal distance between the main wing and the first flap X_1, it can be seen that the factor that has the greatest influence on the value of lift and the value of lift drag ratio is the angle of attack of the second flap θ_2, so the value of lift can be adjusted by changing. Therefore, the adjustment of the lift value can be achieved by changing the angle of attack θ_2 of the second flap.

2.3 Response surface modelling and error analysis

When nonlinearity is observed between the response surface and the independent variables, a higher-order polynomial fit is required. If a third-order or higher-order polynomial fit is used, the phenomenon of lunging may occur, and the computational cost increases exponentially with the increase of the number of variables. In engineering practice, the second-order response surface model is mostly used. The functional expression of the second-order response surface model is:

$$Y = a_0 + \sum_{i=1}^{n} a_i x_i + \sum_{i=1}^{n} a_{ii} x_i^2 + \sum_{ij(i<j)} a_{ij} x_i x_j + \varepsilon \quad i, j = 1, 2, 3, ..., n \tag{1}$$

where n is the total number of independent variables, x_i, x_j is the independent variable, a is the polynomial coefficient and ε is the error term, then equation (1) is transformed into a multiple linear regression equation, and the linear regression model for multiple design variables is:

$$Y = \beta_0 + \beta_1 x_1 + \cdots + \beta_n x_n + \varepsilon \tag{2}$$

Writing equation (2) in matrix form, such that:

$$Y = \begin{bmatrix} y_1 \\ y_2 \\ \vdots \\ y_n \end{bmatrix}, \beta = \begin{bmatrix} \beta_1 \\ \beta_2 \\ \vdots \\ \beta_n \end{bmatrix}, \varepsilon = \begin{bmatrix} \varepsilon_1 \\ \varepsilon_2 \\ \vdots \\ \varepsilon_n \end{bmatrix}, X = \begin{bmatrix} 1 & x_{11} & \cdots & x_{1m} \\ 1 & x_{21} & \cdots & x_{2m} \\ \vdots & \vdots & \vdots & \vdots \\ 1 & x_{n1} & \cdots & x_{nm} \end{bmatrix} \tag{3}$$

Then the multiple linear regression models can be expressed as:

$$Y = X\beta + \varepsilon \tag{4}$$

Unknown coefficient vector β by least squares method:

$$\beta = \left(X^T X\right)^{-1} X^T Y \tag{5}$$

Taking the angle of attack θ_1 of the first flap, the angle of attack θ_2 of the second flap, the horizontal distance X_1 between the main wing and the first flap, the vertical distance Y_1 between the main wing and the first flap, the horizontal distance X_2 between the first flap and the second flap, and the vertical distance Y_2 between the first flap and the second flap in Table 2 as design variables, and the values of L_f lift and L/D lift-to-drag ratio as target values, the second-order response surface model is constructed as follows:

$$\begin{cases} L_f = Z_{lf}{}^T u \\ L/D = Z_{ld}{}^T u \end{cases} \tag{6}$$

where L_f is the lift value; L/D is the lift to resistance ratio, Z_{lf}, Z_{ld} is the coefficient vector and u is the basis function vector.

To detect the error of the response surface model, this paper uses R^2 analysis with the expression:

$$R^2 = \frac{SS_R}{SS_{\mathrm{r}}} \tag{7}$$

Which

$$SS_R = \sum_{i=1}^{n} \left(\hat{y}_i - \overline{y}\right)^2, SS_E = \sum_{i=1}^{n} \left(y_i - \hat{y}_i\right)^2 \tag{8}$$

$$SS_r = SS_R + SS_E \tag{9}$$

where SS_R is the regression sum of squares and SS_E is the residual sum of squares.

In this paper, by randomly selecting 10 points as error analysis points for analysis, the results of R^2 analysis are shown in Table 5, it can be seen that the R^2 of lift force value L_f is greater than 0.9 and the R^2 of lift drag ratio L/D is close to 0.9, so this second-order response surface model has a high degree of confidence.

Table 5 R^2 analysis

Variables	*Lift value*	*Lift drag ratio*
R^2	0.94523	0.89263

3 iSIGHT-based optimisation of aerodynamic characteristics of racing rear wings

As an important source of lift for the racing car, the factors affecting its aerodynamic performance are not only related to the airfoil selection, but also related to the angle of attack of the main wing and flaps and the gap size between the airfoils. Based on the orthogonal test, multi-objective optimisation of the structural parameters of the combined wing space arrangement is carried out based on the iSIGHT software using a parametric approach to determine the optimal range of angle of attack variation between the flaps and the clearance between adjacent flaps for the tailplane under the straight-line racing conditions. The established response surface model is used to optimise the design with the lift and lift-to-drag ratio as the design objectives and the tailplane spatial structure parameters as the design variables.

3.1 Multi-objective genetic algorithm optimisation method

In the optimisation design process, the first flap angle of attack θ_1, the second flap angle of attack θ_2, the horizontal distance between the main wing and the first flap X_1, the vertical distance between the main wing and the first flap Y_1, the horizontal distance between the first flap and the second flap X_2, and the vertical distance between the first flap and the second flap Y_2 are used as design variables, and the lift value D_f and the lift drag ratio are used as design objectives and the desired target aerodynamic characteristics. The target values of D_f and L/D are 500 N/m and –4.8 N/m, respectively, and the mathematical model is established as follows:

$$\begin{cases} \max \ F1 = \left| D_f - 100 \right| \\ \max \ F2 = \left| L/D - 0.5 \right| \\ s.t. \quad 10 \le \theta_1 \le 30 \\ \qquad 20 \le \theta_2 \le 60 \\ \qquad 22 \le X_1 \le 30 \\ \qquad 8 \le Y_1 \le 16 \\ \qquad 12 \le X_2 \le 20 \\ \qquad 6 \le Y_2 \le 14 \end{cases} \tag{10}$$

The optimisation calculation was performed using the constructed second-order response surface model, and the data results from the orthogonal tests were imported into the Approximation model established in iSIGHT, and the NSGA-II algorithm was used for optimisation iterations, the process of which is shown in Figure 6.

Figure 6 iSIGHT optimisation process (a) input of rear wing space structure parameters (b) rear wing optimisation iterative process

General | Variables | Constraints | Objectives

	Parameter	Lower Bound	Value	Upper Bound
☑	X1	10.0	18.0	30.0
☑	X2	20.0	36.0	60.0
☑	X3	22.0	24.0	30.0
☑	X4	8.0	10.0	16.0
☑	X5	12.0	14.0	20.0
☑	X6	6.0	6.0	14.0

(a)

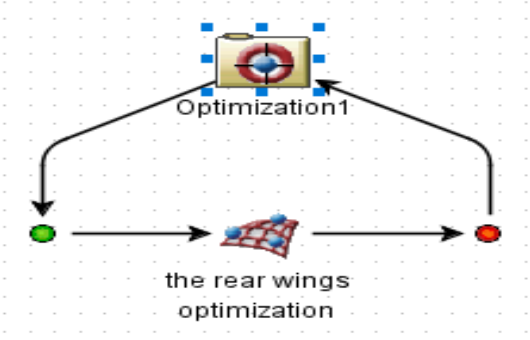

(b)

After 481 iterations of calculation and finally obtaining the solution of the objective function in the 389th iteration, the target lift and lift drag ratio values and the corresponding values of the optimisation variables can be calculated as: The angle of attack of the first flap is $\theta_1 = 20.167°$, the angle of attack of the second flap is θ_2=39.588°, the horizontal distance between the main wing and the first flap is $X_1 = 25.893$ mm, the vertical distance between the main wing and the first flap is $Y_1 = 15.62$ mm, the horizontal distance between the first flap and the second flap is $X_2 = 16.047$ mm, the vertical distance between the first flap and the second flap is Y_2=9.8119 mm, the lift value is $L_f = -500.89$ N, and the lift-to-drag ratio is $L/D = -4.5286$. The calculation results are rounded to the final result, θ_1=20°, θ_2=40°, $X_1 = 25.89$ mm, $Y_1 = 15.62$ mm, X_2=16.05 mm, Y_2=9.82 mm and the lift value is $L_f = -500.89$ N and the lift-to-drag ratio is $L/D = -4.53$.

3.2 Simulation verification of optimisation results

The optimised values in iSIGHT software were imported into ANSYS WorkBench for setting the angle of attack and adjusting the clearance between the airfoils, using ICEM for non-structural meshing, setting its boundary conditions and initial velocity and other parameters in FLUENT and finally obtaining its simulation values as shown in Table 6.

Table 6 Comparison of optimisation results and simulation results

Projects	*Lift value*	*Lift drag ratio*
Target value	–500	–4.8
Fitted value	–500.19	–4.53
Simulation value	–483.24	–4.67
Error value	3.39%	3.09%

The results of the simulation in ANSYS WorkBench are –483.24 N and –4.67. The errors are 3.39% and 3.09%, respectively. According to the experience, the error is within ±5%, which meets the experimental requirements. Therefore, the simulation accuracy meets the requirements.

4 Racing car variable rear wing control system design

4.1 Variable rear wing system principle

When a racing car turns on a wet road at a high speed, the centrifugal force will cause a lateral tilt resulting in the outside wheels of the curve breaking through the adhesion limit, thus making the racing car extremely susceptible to the danger of sideslip or even roll over. To prevent the above-mentioned dangerous situation, a variable rear wing system is proposed, in which the first flap and the second flap of the original wing are disconnected from the middle endplate is fixed on the main wing, and the racing car with this variable rear wing system is shown in Figure 7. By controlling the size of the flap angle of attack, the left and right flaps are turned at different angles to produce different aerodynamic effects on the left and right sides of the wing to generate different downforce, which in turn regulates the size of the positive pressure on the left and right sides of the wheels. The pressure difference generates a return moment opposite to the lateral tilting moment, which reduces the pressure difference between the left and right wheels caused by high-speed turning to suppress the vehicle's lateral tilting and improve the handling stability of the car. At the same time, because the aerodynamic drag generated by the left and right flaps are also different, the rear wing to form the aerodynamic drag difference, can produce the same turning direction of the auxiliary torque, can reduce the car to a higher speed cornering understeer phenomenon, to further improve the handling stability and driving safety of the car.

Figure 7 Variable rear wing racing car 3D model

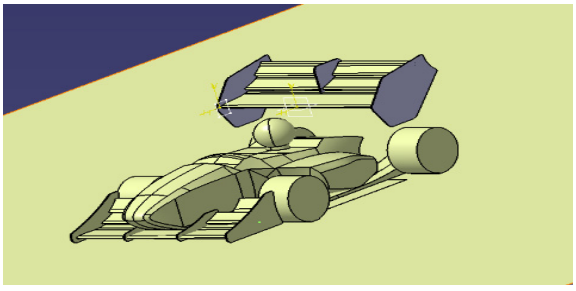

4.2 Derivation of linear reference model for racing car variable rear wing system

The dynamics model of the racing car is simplified, the role of the suspension and the influence of other factors are ignored in the analysis; the influence of the steering system is ignored, the front wheel turning angle is directly used as input and the model of the racing car is simplified to a two-degree-of-freedom bicycle model, i.e., the speed of the car in the *Z*-axis direction is zero, the pitch angle around the *Y*-axis is zero and the lateral tilt angle around the *X*-axis is zero, through the dynamics derivation of the linear two-degree-of-freedom model. Establish the stability parameters that can reflect the state of the racing car. The linear reference model of the car with the variable rear wing system installed is shown in Figure 8.

Figure 8 Racing linear reference model

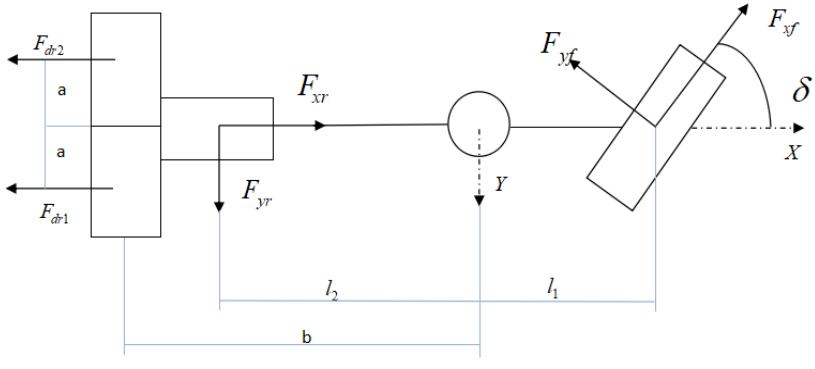

From Figure 8, the sum of the component forces along the *y*-axis and the moments around the centre of mass for the external forces on the linear racing model is:

$$\begin{cases} \sum F_Y = F_{yr} + F_{yf} \\ \sum M_Z = l_1 F_{yf} - l_2 F_{yr} + a\left(F_{dr1} - F_{dr2}\right) \end{cases} \tag{11}$$

Which

$$\begin{cases} F_{yf} = F_{y1} + \mu F_{Z1} \sin \alpha_1 \\ F_{yr} = F_{y2} + \mu F_{Z2} \sin \alpha_2 \end{cases} \tag{12}$$

That is, the differential equation of motion for the linear model of racing is given by:

$$m\left(\dot{V}_y + V_x \Omega_z\right) = \left(F_{y1} + \mu F_{Z1} \sin \alpha_1\right) + \left(F_{y2} + \mu F_{Z2} \sin \alpha_2\right) \tag{13}$$

$$I_Z \dot{\Omega}_Z = l_1\left(F_{y1} + \mu F_{Z1} \sin \alpha_1\right) - l_2\left(F_{y2} + \mu F_{Z2} \sin \alpha_2\right) + a\left(F_{dr1} - F_{dr2}\right) \tag{14}$$

where F_{y1}, F_{y2} are the front and rear wheel lateral deflection forces; α_1, α_2 are the front and rear wheel lateral deflection angles; F_{z1}, F_{z2} are the downforce acting on the front and rear axles respectively; F_{dr1}, F_{dr2} are the aerodynamic drag forces acting on the left and right rear wings, respectively μ is the ground and tyre friction coefficient, l_1, l_2 are the distance between the centre of mass of the car and the front and rear axles, respectively; m is the mass of the car, I_z is the rotational inertia of the car around the centre of mass; V_y is the lateral velocity of the car; V_x is the longitudinal velocity of the car; Ω_z is the angular velocity of the transverse oscillation of the car.

where the tyre lateral force is:

$$F_{y1} = C_f \alpha_1 \tag{15}$$

$$F_{y2} = C_r \alpha_2 \tag{16}$$

$$\alpha_1 = \delta - \left(V_y + a\Omega_z\right) \Big/ V_x \tag{17}$$

$$\alpha_2 = \left(V_y + b\Omega_z\right) \Big/ V_x \tag{18}$$

where C_f and C_r are the lateral deflection stiffness of the front and rear tyres, respectively.

The aerodynamic drag and downforce on the rear wing is:

$$F_{dri} = \frac{C_D \rho V_x^2 A_w \sin \theta_i}{2} \tag{19}$$

$$F_{li} = \frac{C_L \rho V_x^2 A_w \cos \theta_i}{2} \tag{20}$$

where C_L and C_D are the wing lift and drag coefficients, respectively; ρ is the air density; A_ω is the windward area of the tail; $\theta_i \left(i = 1, 2\right)$ represents the left and right-wing flap angle of attack. When the angle of attack of the left and right flaps are different, it will cause the left and right-wing to produce different downforce acting on the left and right wheels, which will create the problem of downforce distribution and the downforce produced by the variable rear wing acts on the front and rear axles of the racing car, as shown in Figure 9.

Figure 9 Variable rear wing downforce distribution

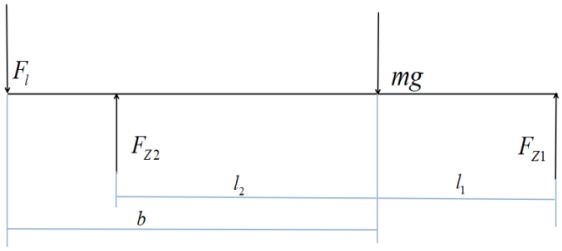

From Figure 9, it can be seen that the rear wing acts on the upper and lower pressures on the front and rear axles, respectively, expressed as:

$$F_{Z1} = m\left(\frac{l_2}{l_1 + l_2}\right) - F_l\left(\frac{b - l_2}{l_1 + l_2}\right) \tag{21}$$

$$F_{Z2} = m\left(\frac{l_2}{l_1 + l_2}\right) + F_l\left(\frac{b + l_1}{l_1 + l_2}\right) \tag{22}$$

$$F_l = F_{l1} + F_{l2} \tag{23}$$

5 Hybrid fuzzy PID control strategy design

A hybrid fuzzy PID control strategy is designed for active control of a racing car variable rear wing system. The ideal transverse swing angle speed output from the reference model is compared with the actual transverse swing angle speed output from CarSim by taking the front wheel turning angle as input, and then the error and error change rate are input to the fuzzy controller, which can effectively reduce the fluctuation range of angle of attack change and effectively improve the control accuracy and response speed of angle of attack by connecting a PID controller in parallel. The second flap angle of attack is set to be twice the first flap angle of attack, and then the aerodynamic drag and downforce are calculated based on the obtained flap angle of attack and input to the CarSim racing car model to realise the joint simulation. The block diagram of the designed racing car variable rear wing control system is shown in Figure 10.

The hybrid fuzzy PID controller is composed of a 2D fuzzy controller and a conventional PID controller in parallel, and takes the difference between the actual transverse swing angular velocity of the race car and the ideal transverse swing angular velocity and the rate of change of the difference as the input of the hybrid fuzzy PID controller, and the angle of attack θ of the rear wing as the output. The fuzzy controller is a two-dimensional controller with two inputs and a single output, the theoretical range of the angular velocity error E of the transverse pendulum is [–0.5 0.5], the unit is rad/s, the theoretical range of the error rate of change EC is [–0.5 0.5] and the theoretical range of the output U is the angle of attack θ of the first flap of the wing is [–0.399 0.399] in rad. The quantisation levels of all three are set to 7: NB (negative large), NM (negative medium), NS (negative small), ZO (zero), PS (positive small), PM (positive medium) and PB (positive large). That is, the three affiliation functions are shown in Figure 11.

Figure 10 Block diagram of racing car variable rear wing control system

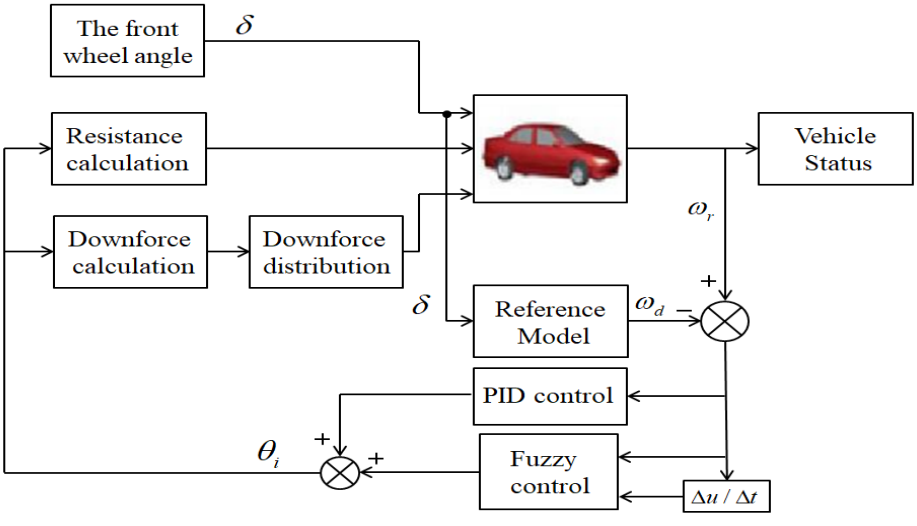

Figure 11 Affiliation function (a) The affiliation functions of the input quantities E and EC (b) The affiliation function of the output quantity U

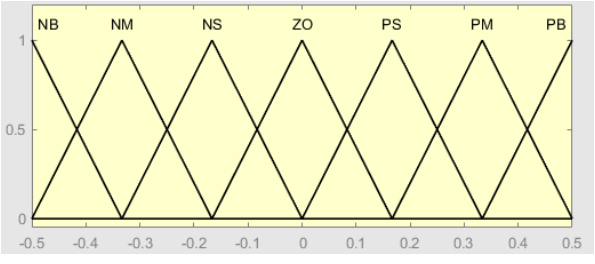

(a)

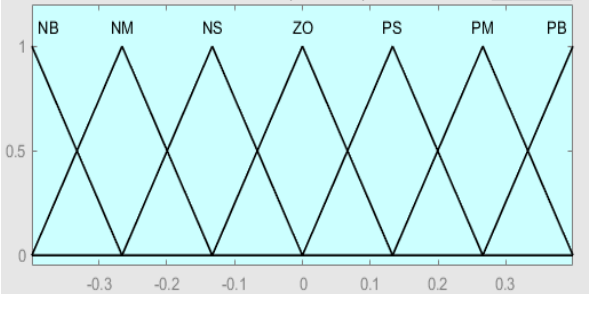

(b)

Based on the analysis of the variable rear wing control system and the actual working conditions of the racing car driving, the fuzzy control fuzzy rules are designed and the fuzzy control rules are shown in Table 7.

Table 7 Fuzzy control rules table

θ		*EC*						
		NB	*NM*	*NS*	*ZO*	*PS*	*PM*	*PB*
E	NB	PB	PB	PB	PB	PM	PS	ZO
	NM	PB	PB	PB	PM	PS	ZO	NS
	NS	PB	PB	PM	PS	ZO	NS	NM
	ZO	PB	PM	PS	ZO	NS	NM	NB
	PS	PM	PS	ZO	NS	NM	NB	NB
	PM	PS	ZO	NS	NM	NB	NB	NB
	PB	ZO	NS	NM	NB	NB	NB	NB

The observed fuzzy rule surface for the angular velocity of the transverse pendulum is obtained as shown in Figure 12.

Figure 12 Output curve of the observed fuzzy rule for the angular velocity of the transverse pendulum

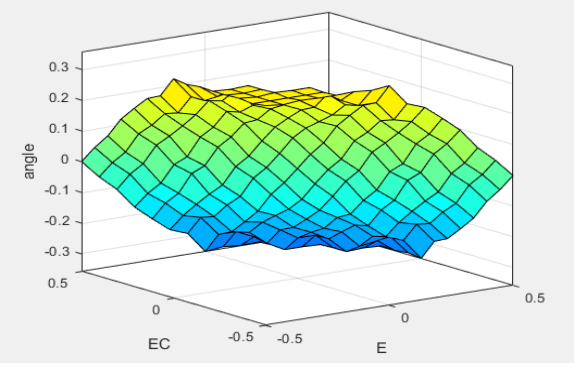

6 Simulation analysis

The parameters of the racing car model are shown in Table 8. Based on the joint simulation platform of MATLAB/Simulink and CarSim, the transverse angular velocity, the lateral deflection angle of the centre of mass, lateral velocity and lateral acceleration of the race car were selected as the evaluation indexes of the handling stability of the race car, and the effectiveness of the control system was verified and analysed under single-shift line conditions, the same vehicle speed V=72 km/h and different ground adhesion coefficients $\mu = 0.7, \mu = 0.6, \mu = 0.5$ (Hu et al., 2021). The three adhesion coefficients represent concrete pavement, asphalt pavement and pavement with partial snow or relatively slippery surface, respectively.

Table 8 Racing car parameters

Parameters	*Value*
Overall vehicle mass m_v / kg	220
Driver Quality m_d/kg	70
Distance from the side-slip angle to the front axle l_1 / mm	1125
Distance from the side-slip angle to the rear axis l_2 / mm	1550
Total aerodynamic kit mass m_a / kg	15
Road adhesion coefficient μ	0.7/0.6/0.5
Inertia moment of mass about the vertical axis I_Z / (kg×m^2)	1500
Front-wheel lateral deflection stiffness $C_f\left(N/rad\right)$	30000
Rear-wheel lateral deflection stiffness $C_r\left(N/rad\right)$	30000
Air Density $\rho/\left(\text{kg}\times\text{m}^3\right)$	1.225

1) When the ground adhesion coefficient μ=0.7, the transient response comparison curve of the racing car is shown in Figure 13.

Figure 13 $\mu=0.7$ racing transient response curve (a) Time history comparison curve of yaw rate (b) Time history comparison curve of side-slip angle (c) Time history comparison curve of lateral acceleration (d) Time history comparison curve of lateral speed

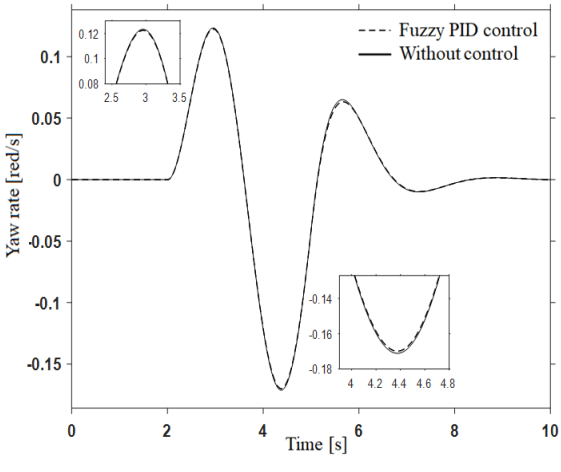

(a)

Figure 13 $\mu = 0.7$ racing transient response curve (a) Time history comparison curve of yaw rate (b) Time history comparison curve of side-slip angle (c) Time history comparison curve of lateral acceleration (d) Time history comparison curve of lateral speed (continued)

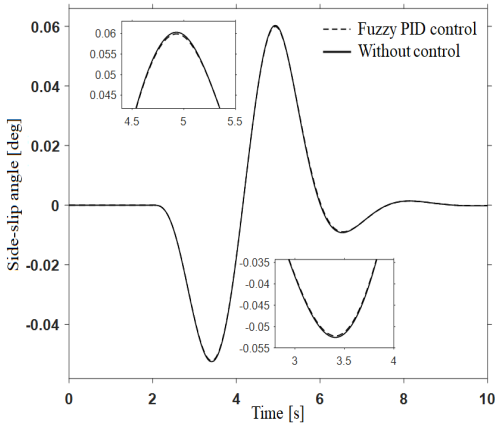

(b)

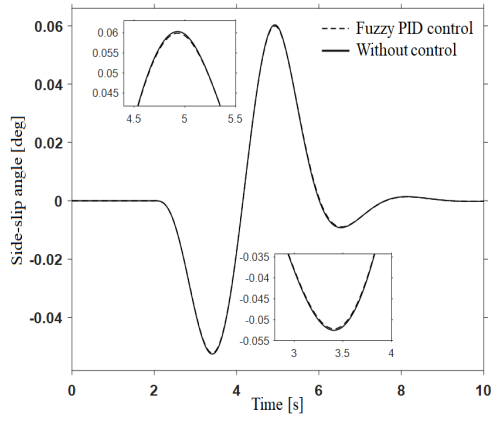

(c)

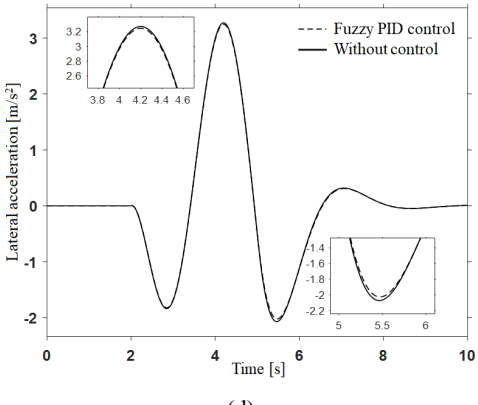

(d)

The variable rear wing control system has no significant effect on the handling stability of the car when the ground adhesion coefficient is μ=0.7 concrete pavement.

2) When the ground adhesion coefficient μ=0.6, the transient response comparison curve of the racing car is shown in Figure 14.

Figure 14 $\mu = 0.6$ racing transient response curve (a) Time history comparison curve of yaw rate (b) Time history comparison curve of side-slip angle (c) Time history comparison curve of lateral acceleration (d) Time history comparison curve of lateral speed

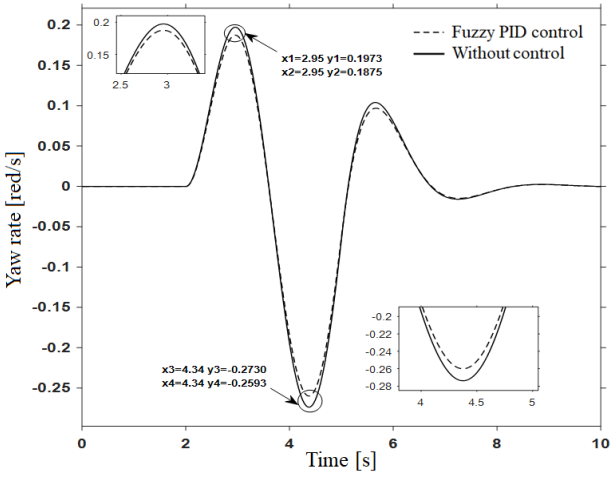

(a)

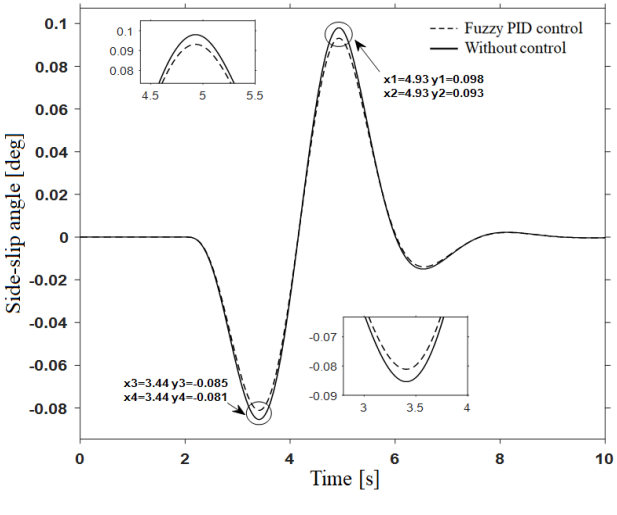

(b)

Figure 14 $\mu = 0.6$ racing transient response curve (a) Time history comparison curve of yaw rate (b) Time history comparison curve of side-slip angle (c) Time history comparison curve of lateral acceleration (d) Time history comparison curve of lateral speed (continued)

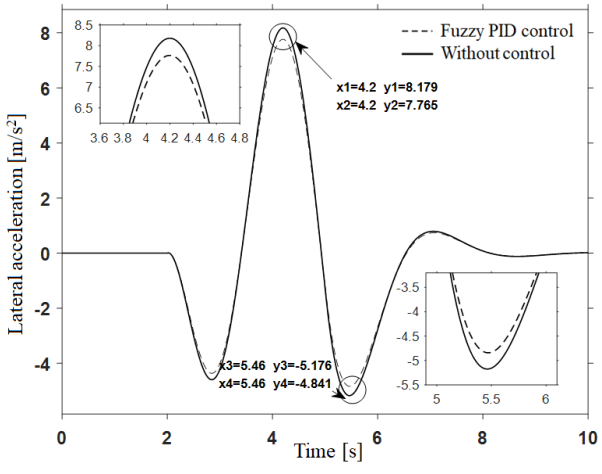

(c)

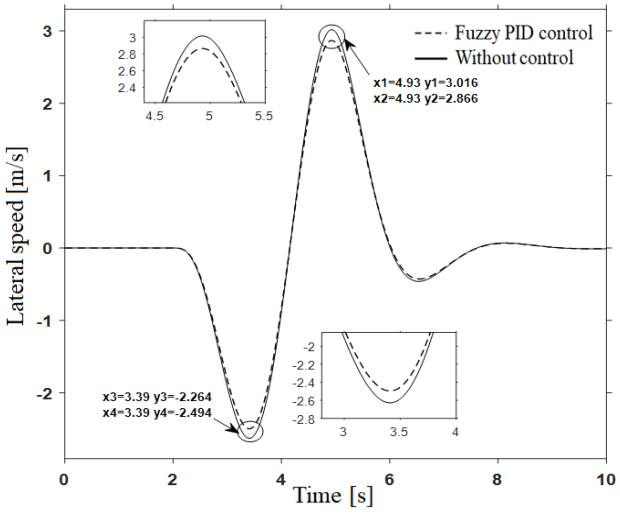

(d)

When the ground adhesion coefficient μ=0.6 asphalt pavement, with or without variable rear wing system has a certain influence on the peak of the evaluation index of racing car handling stability, the peak of transverse swing angular velocity changed from -0.273 rad/s to -0.259 rad/s , a decrease of 5.13%, the peak of mass lateral deflection angle changed from 0.098 deg to 0.093 deg , a decrease of 5.10%, the peak of lateral acceleration changed from 8.179 m/s^2 to 7.765 m/s^2, a reduction of 5.06% and the peak

lateral velocity changed from 3.016 m/s to 2.866 m/s, a reduction of 4.97%. The variable rear wing system improves the handling stability of the car to a certain extent.

3) When the ground adhesion coefficient μ=0.5, the transient response comparison curve of the racing car is shown in Figure 15.

Figure 15 $\mu = 0.5$ racing transient response curve (a) Time history comparison curve of yaw rate (b) Time history comparison curve of side-slip angle (c) Time history comparison curve of lateral acceleration (d) Time history comparison curve of lateral speed

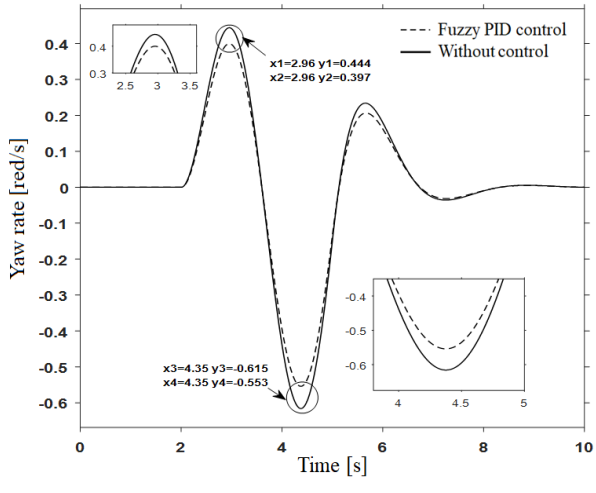

(a)

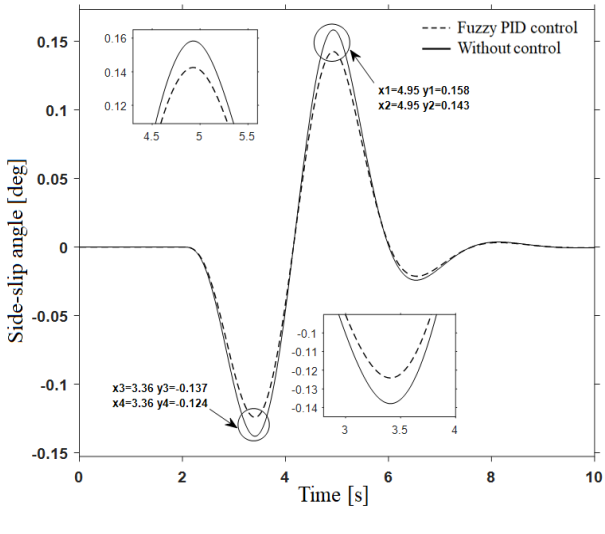

(b)

Figure 15 $\mu = 0.5$ racing transient response curve (a) Time history comparison curve of yaw rate (b) Time history comparison curve of side-slip angle (c) Time history comparison curve of lateral acceleration (d) Time history comparison curve of lateral speed (continued)

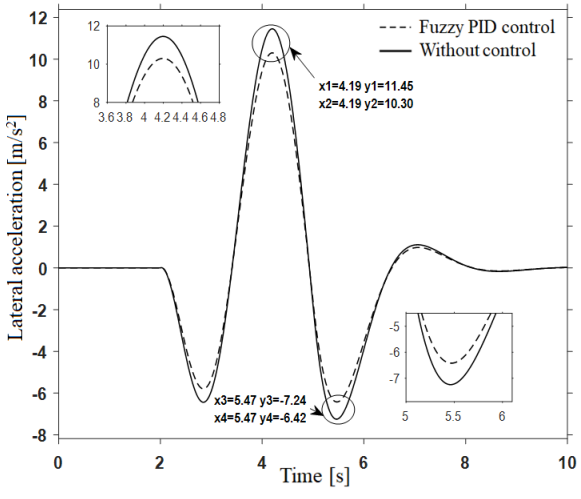

(c)

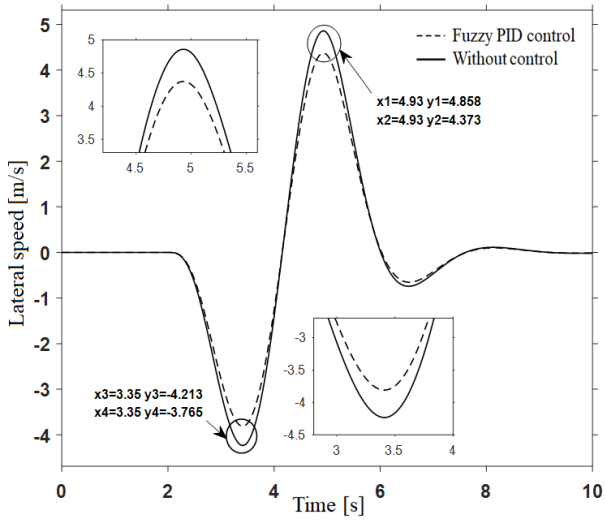

(d)

When the ground adhesion coefficient μ=0.5 A has some snow or relatively slippery surface, the presence or absence of a variable rear wing system has a greater impact on the peak of the evaluation index of the car's handling stability. The peak transverse swing angular velocity changes from -0.615 rad/s to -0.553 rad/s , a decrease of 10.08%, the peak mass lateral deflection angle changes from 0.158 deg to 0.143 deg , a decrease of 9.49% and the peak lateral acceleration changes from 11.451 m/s^2 to 10.382 m/s^2, a

decrease of 9.34%. The peak lateral velocity changed from 3.016 m/s to 2.866 m/s, a decrease of 9.88%. The variable rear wing system has significantly improved the handling stability of the car.

The changes in the peak values of the evaluation indicators are shown in Table 9.

Table 9 Comparison of peak evaluation indexes under different pavement adhesion coefficients

	Parameters	*Yaw rate (rad/s)*	*Side-slip angle (deg)*	*Lateral acceleration (m/s^2)*	*Lateral speed (m/s)*
μ=0.5	Fuzzy PID control	–0.553	0.143	10.382	4.373
	Without control	–0.615	0.158	11.451	4.858
μ=0.6	Fuzzy PID control	–0.259	0.093	7.765	2.866
	Without control	–0.273	0.098	8.179	3.016
μ=0.7	Fuzzy PID control	–0.170	0.062	3.203	1.481
	Without control	–0.171	0.060	3.204	1.483

Under the same speed conditions, as the ground adhesion conditions gradually deteriorate, to suppress the vehicle's sway phenomenon in the cornering conditions, the variable rear wing system makes the difference between the left and right flap angle of attack gradually become larger, so that the inner wheels gradually get more downforce to reduce the pressure difference between the left and right wheels, the suppression effect on the vehicle sway is gradually strengthened and the peak of the handling stability evaluation index gradually becomes smaller. With the variable rear wing system, cornering performance is improved, as well as handling stability and driving safety on snowy or relatively slippery roads.

7 Conclusions

1) Multi-objective optimisation of the tailplane based on orthogonal tests and the iSIGHT platform was carried out to determine the optimal combination of the angle of attack of the tailplane flaps and the optimal relative clearance between adjacent flaps, and the optimisation results were verified to meet the experimental requirements.

2) To further improve the handling stability of the racing car under turning conditions on wet roads, a variable rear wing control system is proposed and a hybrid fuzzy PID variable rear wing system controller is designed to track the ideal transverse swing angular velocity strategy.

3) Based on the joint simulation platform of Matlab/Simulink and CarSim, the effectiveness of the variable rear wing system was simulated and analysed. The results show that the improvement effect on the handling stability of the car is more significant under the condition of partial snow or relatively slippery road surface. With the deterioration of road surface adhesion conditions, the improvement of overall vehicle handling stability becomes more and more obvious, which significantly improves the cornering performance and driving safety of the car.

Acknowledgements

Financial support of this research by the National Natural Science Foundation of China (grant number 52072116), Key Laboratory of Automotive Power Train and Electronics (Hubei University of Automotive Technology) (grant nos. 2015XTZX04, 2015XTZX0423, 2015XTZX0424) and key research and development Projects in Hubei Province (grant no. 2020BAB141). Hubei Provincial Education Department Research Project (grant nos. B2021143, B2021144). 2021 Outstanding graduate student dissertation cultivation project (grant no. Y202127).

References

Ayyagari, D.T. and He, Y. (2017) 'Aerodynamic analysis of an active rear split spoiler for improving lateral stability of high-speed vehicles', *International Journal of Vehicle Systems Modelling and Testing*. Doi: 10.1504/IJVSMT.2017.089978.

Deng, Z., Gao, W., Wu, C., Li, P. and Chen, M. (2016) 'Development of adjustable wing control system prototype for FSAE racing car', *Journal of Hefei University of Technology (Natural Science Edition)*, Vol. 4, pp.445–450.

Diba, F. et al. (2014) 'Handling and safety enhancement of race cars using active aerodynamic systems', *Vehicle System Dynamics*, Vol. 52, No. 9. Doi:10.1080/00423114.2014.930158.

Diba, F. et al. (2014) 'Handling and safety enhancement of race cars using active aerodynamic systems', *Vehicle System Dynamics*, Vol. 52, No. 9. Doi:10.1080/00423114.2014.930158.

Hammad, M. (2019) *Design and Analysis of Active Aerodynamic Control Systems for Increasing the Safety of High-Speed Road Vehicles*, University of Ontario Institute of Technology, Oshawa.

Hammad, M., Qureshi, K. and He, Y. (2019) 'Safety and lateral dynamics improvement of a race car using active rear wing control', *SAE Technical Paper*. Doi: 10.4271/2019-01-0643.

He, Y. (2013) 'Design of an actively controlled aerodynamic wing to increase high-speed vehicle safety', *SAE Technical Paper*. Doi: 10.4271/2013-01-0802.

He, Y. et al. (2013) 'Aerodynamic characteristics of the rear lift wing of a Formula 1 car', *Journal of Aerodynamics*, Vol. 28, No. 10, pp.2343–2347. Doi: 10.13224/j.cnki.jasp.2013.10.030.

Hu, L., Luo, S., Yang, Q. and Yang, S. (2015) 'Aerodynamic kit design for university formula racing car', *Journal of Wuhan University of Science and Technology*, Vol. 38, No. 5, pp.377–380.

Hu, W., Zhang, X., Li, X. and Chen, S. (2021) 'Research on the optimal distribution algorithm of braking force variable ratio for electric vehicles considering the influence of road adhesion conditions', *Mechanical Science and Technology*, Vol. 40, No. 2, pp.296–304. Doi: 10.13433/j.cnki.1003-8728.20200034.

Li, L. (2015) 'Design rules for the formula student racing car competition', *Chinese Society of Automotive Engineering*.

Liu, C. (2018) *Analysis and Optimization of Aerodynamic Characteristics of an FSC Racing Car*, Hunan University, Changsha.

Ni, J., Wu, C-C. and Chen, S-Z. (2012) 'Virtual experiment on the effect of rear wing attack angle variation on the performance of a formula car', *Mechanical Design and Research*, Vol. 28, No. 2, pp.96–99.

Wan, T.T. (2018) *Research on the Control Strategy of Adjustable Wing System of FSE Electric Racing Car*, Guangdong University of Technology, Guangzhou.

Xu, Z.M., Yu, F., Zhang, Z.F., Su, Z.C. and He, Y.N.S. (2009) 'Stability control modeling and simulation of vehicle turning and braking dynamics', *Journal of System Simulation*, Vol. 21, No. 13, pp.4135–4139.

Yang, Z., Gu, W. and Li, Q. (2011) 'Aerodynamic design optimization of race car rear wing', *Proceedings of IEEE International Conference on Computer Science and Automation Engineering*, Institute of Electrical and Electronics Engineers, Inc., pp.666–670.

Yu, K. and Xie, S. (2018) 'CFD-based design and optimization study of FSAE racing rear wings', *Mechatronics Engineering*, Vol. 35, No. 1, pp.16–21.

Zhang, W., Wang, J. and Ji, Z. (2018) 'Design and testing of wing drag reduction system for university formula racing cars', *Mechanical Design and Research*, Vol. 34, No. 6, pp.202–204.

Zhu, F. (2017) *Analytical Study on Aerodynamic Characteristics of FSC Racing Car Body*, North Central University.